Time-domain induced polarization as a tool to image clogging in treatment wetlands

R Garcia-Artigas, M Himi, A Revil, A Urruela, R Lovera, A Sendrós, A Casas, L Rivero

Science of the Total Environment 724 (2020) 138189

Contents lists available at ScienceDirect

Science of the Total Environment

journal homepage: www.elsevier.com/locate/scitotenv

Time-domain induced polarization as a tool to image clogging in treatment wetlands

R. Garcia-Artigas [a,b], M. Himi [b], A. Revil [c,*], A. Urruela [b], R. Lovera [a,b], A. Sendrós [a,b], A. Casas [a,b], L. Rivero [a,b]

[a] Water Research Institute (IdRA), University of Barcelona, 08028 Barcelona, Spain
[b] Mineralogy, Petrology and Applied Geology Department, Faculty of Earth Sciences, University of Barcelona, 08028 Barcelona, Spain
[c] Université Grenoble Alpes, USMB, CNRS, EDYTEM, 73000 Chambéry, France

HIGHLIGHTS

- Time-domain induced polarization is used to image clogging in a constructed wetland.
- A linear correlation between normalized chargeability and the weight percentage of clogging is observed.
- Normalized chargeability as a proxy for clogging is demonstrated and used in the field.

GRAPHICAL ABSTRACT

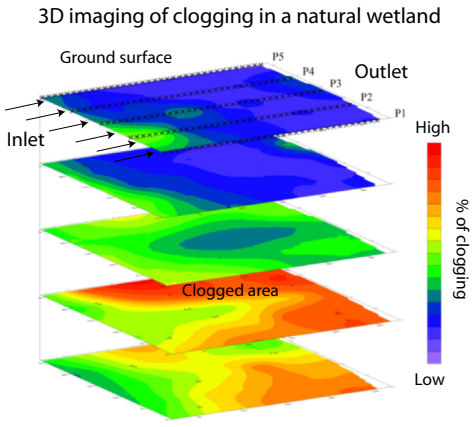

ARTICLE INFO

Article history:
Received 30 January 2020
Received in revised form 18 March 2020
Accepted 23 March 2020
Available online 25 March 2020

Editor: Jose Julio Ortega-Calvo

Keywords:
Chargeability
Treatment wetland
Clogging
Tomography

ABSTRACT

During the last decade, treatment (artificial) wetlands have flourished all over Europe for the treatment of sewages from small communities thanks to their low cost of operation. The clogging of the filter of these wetlands is an issue affecting their efficiency and considered as their main operational problem. The present work shows the results of the application of a geophysical method called time-domain induced polarization. It is used to non-intrusively image, in 3D, the clogging of the gravel filters in a quick and efficient way. Induced polarization characterizes the ability of a porous material to reversibly store electrical charges when submitted to an electrical field. The material property characterizing this ability is called normalized chargeability. A set of laboratory experiments allows to determine an empirical relationship between the normalized chargeability and the weight amount of clogging. Induced polarization measurements have been performed in the field over a treatment wetland to get a 3D reconstructed image (tomography) of the normalized chargeability. From this tomography and the previously defined relationship, we are able to image in 3D the distribution of clogging and where it is concentrated in the filter. We can therefore identify the areas requiring preventive measures to minimize this clogging issue.

* Corresponding author.
E-mail addresses: r.garcia@ub.edu (R. Garcia-Artigas), himi@ub.edu (M. Himi), andre.revil@univ-smb.fr (A. Revil), aritz.urruela@ub.edu (A. Urruela), rlovera@ub.edu (R. Lovera), alex.sendros@ub.edu (A. Sendrós), albert.casas@ub.edu (A. Casas), lrivero@ub.edu (L. Rivero).

https://doi.org/10.1016/j.scitotenv.2020.138189
0048-9697/

1. Introduction

During the last decade, treatment (artificial) wetlands have been developed for the treatment of wastewater of small communities of less than ~2000 people (e.g., Puigagut et al., 2007) as well as for treating industrial wastewaters (e.g. Vymazal, 2014), greywaters (e.g.; Abed et al., 2017), stormwater runoffs (e.g., Headley and Tanner, 2011), and even mine tailings with contamination for instance associated with chromium and nickel (Ranieri and Young, 2012; Ranieri, 2012; Ranieri et al., 2016). Treatment wetlands are engineered systems that have been designed to take advantage of the same filtration processes that occur in natural wetlands after a primary treatment consisting of screening and grit removal (e.g. Vymazal, 2005; Puigagut et al., 2007; Kadlec and Wallace, 2009; Vera et al., 2011). The filtration should be seen first as a physical process in which the organic matter is retained or filtered by the sand and gravel. Then it is undergoing hydrolysis followed by biological degradation. Treatment wetlands may be categorized following their design parameters: Subsurface flow treatment wetlands are subdivided into horizontal flow and vertical flow wetlands depending on the main direction of pore water flow, the ground surface may be vegetated and are generally used for secondary treatment of wastewaters in order to prevent clogging of the filter (e.g. Kadlec and Wallace, 2009; Vymazal, 2011; Dotro et al., 2017). Vertical flow wetlands for treating wastewaters without a primary treatment, the so-called French vertical flow wetlands, have also been introduced and successfully applied to treat wastewaters from small communities. Surface flow treatment wetlands are densely vegetated units, in which the water flows above the media bed and are generally used for tertiary wastewater treatment. In subsurface flow wetlands, the water level is kept below the sand and gravel filter (e.g. Kadlec and Wallace, 2009; Vymazal, 2011; Dotro et al., 2017).

Treatment wetlands act as a biofilter, filtering nutrients, organic matter and pathogens from the wastewaters. Perhaps, it is therefore not surprising that the main problem affecting treatment wetlands is the development of clogging. Clogging, as defined by Pucher and Langergraber (2019), denotes the infilling of the pore space of the filter by fine particles and bacteria/organic matter altering and hindering the movement of both water and contaminants through the filter. Heterogeneity in the development of clogging implies some heterogeneity as well in the local flow velocity distribution and the development of preferential flow paths. In turn, this leads to the exclusion of some subparts of the filter, which are becoming ineffective for the treatment critically reducing the lifetime of the plant (Knowles et al., 2011; Nivala et al., 2012; Pucher and Langergraber, 2019). Clogging includes also the role of inorganic particles (clogging due to suspended solids), mainly proceeding from the wear of the substrate (Matos et al., 2017, 2018; Pucher and Langergraber, 2019) and bioclogging is associated with the development of biofilms, organic matter, and the precipitation of organocomplexes (Pedescoll et al., 2011; Pucher and Langergraber, 2019).

Some approaches have been developed to minimize the development of clogging like the removal of the macrophytes (Pedescoll et al., 2011). There have been many attempts to limit filter clogging. The traditional restoration procedure to a treatment wetland is to remove the clogged bed media and replace it with a clean filter or, if it is a gravel-based system, wash it and return it to the wetland bed. Both approaches are costly and may require sections of the facility to be extruded for some time (Nivala and Rousseau, 2009). In this perspective, chemical treatments to oxidize the organic matter using hydrogen peroxide has appeared as a potential solution to maintain filters (Nivala and Rousseau, 2009), In order to optimize such remediation techniques, we need to visualize both flow paths and clogging.

Existing classical techniques to understand the flow paths include tracer tests (Marzo et al., 2018), solids extraction and measurements of the hydraulic conductivity in a set of piezometers installed in the filter (Marzo et al., 2018; Matos et al., 2019; Licciardello et al., 2019). These methods share a main problem corresponding to the small number of piezometers available. Also these measurements are local, intrusive, and cannot be used to draw maps. A procedure based on the interpretation of thin sections allows understanding the distribution of clogging (Kim and Forquet, 2016). This method, despite being promising, is also invasive.

In this perspective geophysical techniques such as the geo-radar (Tapias et al., 2013; Matos et al., 2019), electrical resistivity tomography (Tapias et al., 2013; Marzo et al., 2018), frequency-domain electromagnetic measurements (Martinez-Carvajal et al., 2020) and X-ray computed tomography (Martinez-Carvajal et al., 2019, 2020) can play a strong role in characterizing the state of the filter regardless the availability of piezometers. In order to be efficient in these approaches, non-intrusive techniques able to quantify clogging would be useful. However, to our knowledge, no geophysical methods to date are able to provide a quantitative idea of the amount of clogging in the subsurface.

Induced polarization is a geophysical technique that can be used to image two key-properties of the subsurface, namely the electrical conductivity and the normalized chargeability. The former refers to the ability to porous media to conduct an electrical current while the second refers to the reversible accumulation of charge carriers (low frequency polarization) under the influence of a primary electrical field (Schlumberger, 1920). Clays and bacteria are coated by an electrical double layer, which is responsible for the polarization of these particles. A recently developed model called the dynamic Stern layer concept (the Stern layer being the inner part of the double layer coating the surface of the grains and bacteria) seems to explain all induced polarization measurements to date made in the laboratory as well as in the field (see Rosen et al., 1993; Revil and Florsch, 2010; Revil, 2012, 2013a).

The motivation for our work is based on the following observations and modelling effort. The dynamic Stern layer model of induced polarization implies that the normalized chargeability is strongly controlled by both the Cation Exchange Capacity (CEC) of clay materials (Revil, 2012, 2013a) and the presence of bacteria (Revil et al., 2012; Zhang et al., 2014). Since clogging materials are expected to have a strong CEC and biofilms are present, imaging the normalized chargeability distribution of treatment wetlands is the key to quantify the amount of clogging in the porous filter. This idea is tested in this work. If we can non-intrusively image clogging, this also means that we can monitor its occurrence, both in space and time, and therefore complete clogging of the porous filter can be anticipated and this would reduce *ipso facto* the cost of maintenance of these treatment wetlands.

2. Materials and methods

An operational wetland located in Vedú (Spain) is used as a test site in the present study. This treatment wetland treats the urban wastewater from Verdú (population of 919 people in 2019), although maximum designed flow rate was 400 m^3/d, the mean flow rate is 150 m^3/day. This waste water treatment system includes a pre-treatment of the waste water consisting on three septic tanks with a volume of 50 m^3 and placed side by side (Fig. 1). The resulting effluent is distributed to four gravel-based horizontal subsurface flow artificial wetlands with a surface area of 977 m^2 for each of them, a 7 day operating/7 day resting cycle, a gravel size for the filter ranging from 6 to 12 mm, and a 40% porosity. The mean inlet Total Dissolved Solid (TDS) concentrations in the pore water ranges between 749 and 96 mg/L. The TDS concentration of the outlet ranges between 66 and 2 mg/L, achieving therefore an average reduction of 96%. Outlet values with mean effluent TDS concentrations of 8.7 ± 5.4 mg/L. are below the threshold of 35 mg/L (a reduction of 90%) as set by the Urban Waste Water Treatment Directive #91/271/EEC. The mean inlet Chemical Oxygen Demand (COD) concentrations in the system ranges from 1020 mg/L to 167 mg/L while at the outlet it ranges from 90 to 26 mg/L achieving an average reduction of 90.5%. Outlet values with mean effluent COD concentrations of 48.5 ±

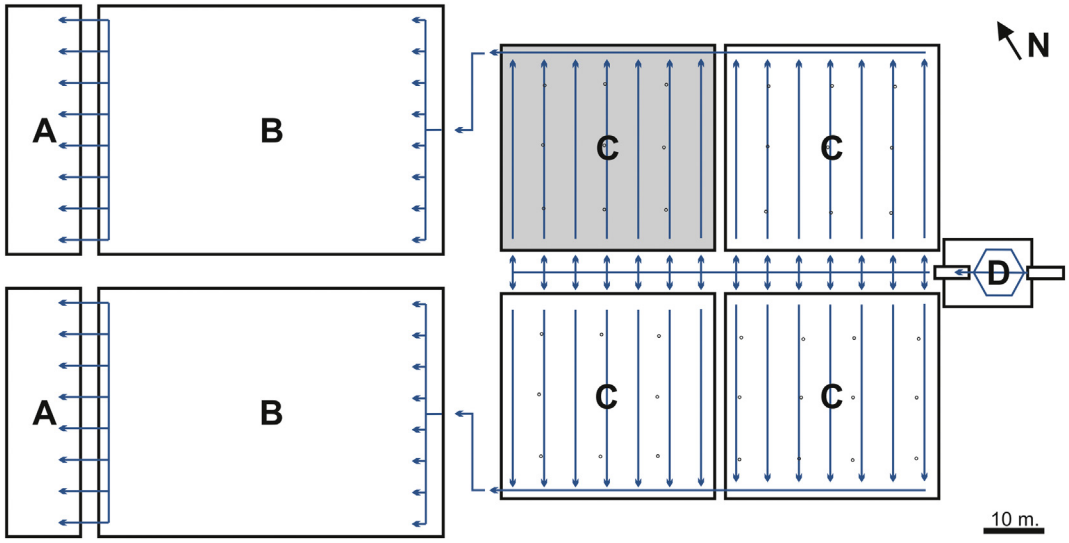

Fig. 1. Verdú horizontal subsurface flow constructed wetland scheme. A; small horizontal subsurface flow constructed wetlands, B; maturation ponds, C; horizontal subsurface flow constructed wetlands and D; pre-treatment stage. The arrows indicate the flow direction. The horizontal subsurface flow constructed wetland is shaded in grey in the filter.

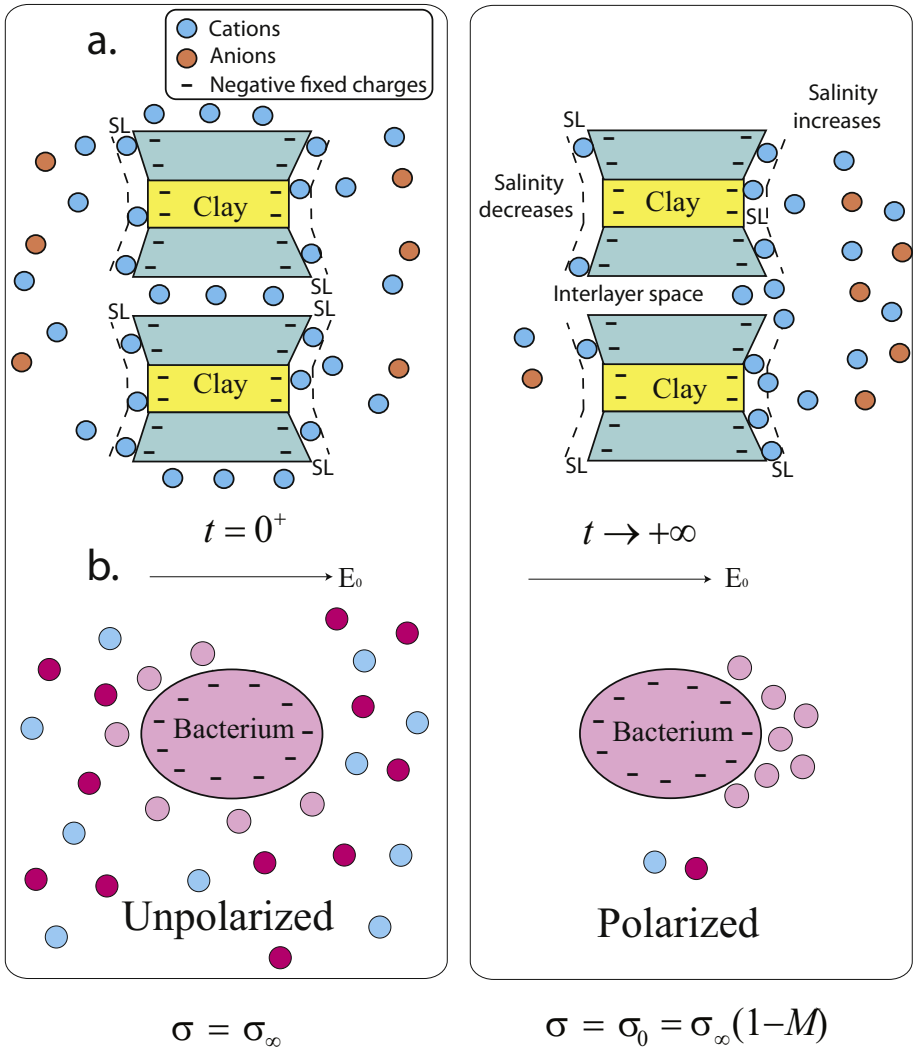

Fig. 2. Clogging can be made of fine particles and biofilms formed by bacteria, a. In an imposed electrical field E_0, Fine particles like here a clay particle get polarized. b. In a similar way, bacteria gets polarized in an applied electrical field. In both cases, the polarized particle behaves like a dipole generating a secondary electrical field, responsible for the observed induced polarization. The short application of the electrical field defines the instantaneous conductivity while a long application of the electrical field defines the Direct Current (DC) conductivity. The difference between the two conductivities defines the normalized chargeability.

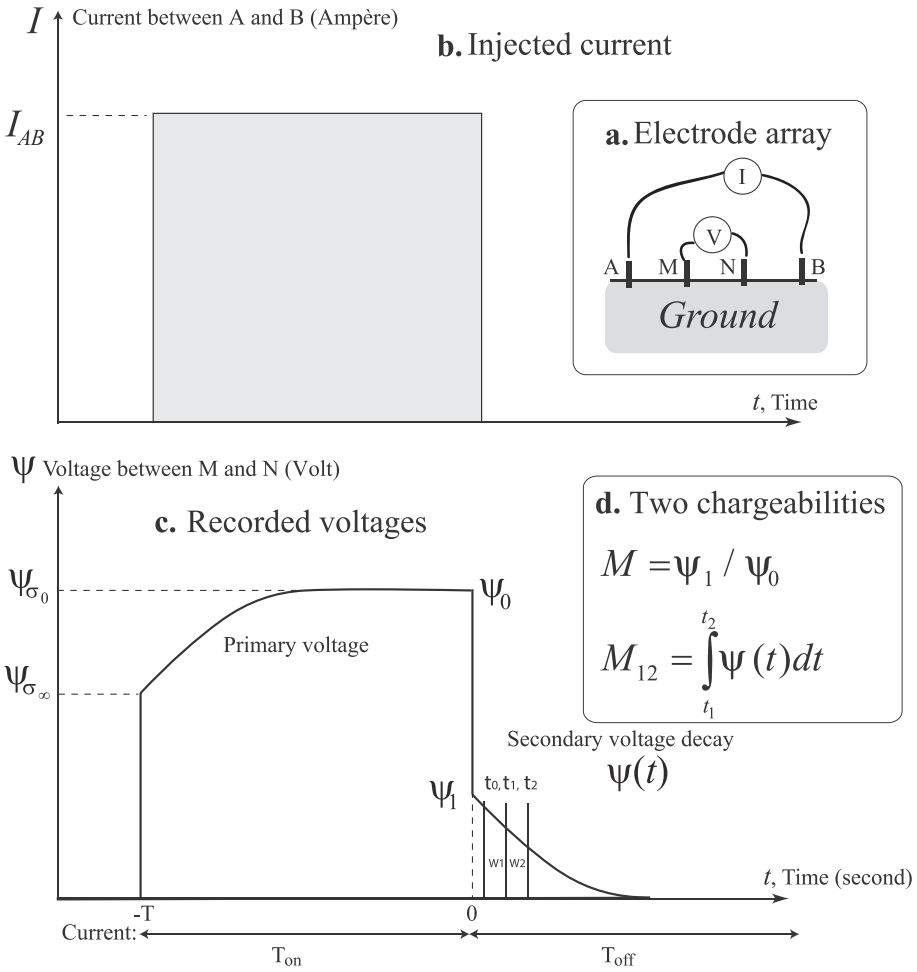

Fig. 3. Classical induced polarization sequence in the time domain, with of two distinct chargeability definitions. a. Electrode array composed of two current electrodes A and B connected to a current generator. Electrodes M and N are the voltage electrodes connected to a voltmeter characterized by a very high input impedance. b. Box current characterized by a period T_{on}. The duration between two current injection, *Toff*, should be large enough to allow a full decay of the secondary voltage otherwise the potential would build up in the ground. c. Recorded voltage difference between the electrodes M and N. The buildup of the voltage and the decay of the secondary voltage are symmetrical. We distinguish an initial voltage buildup ψ_{σ_∞} defining the instantaneous conductivity σ_∞ and a steady-state or direct current (DC) voltage buildup ψ_{σ_0} defining the DC conductivity σ_0. d. Two chargeabilities can be defined. A total chargeability M (dimensionless) and a partial chargeability M_{12} (in s) defined for a given time window during the decay of the secondary voltage.

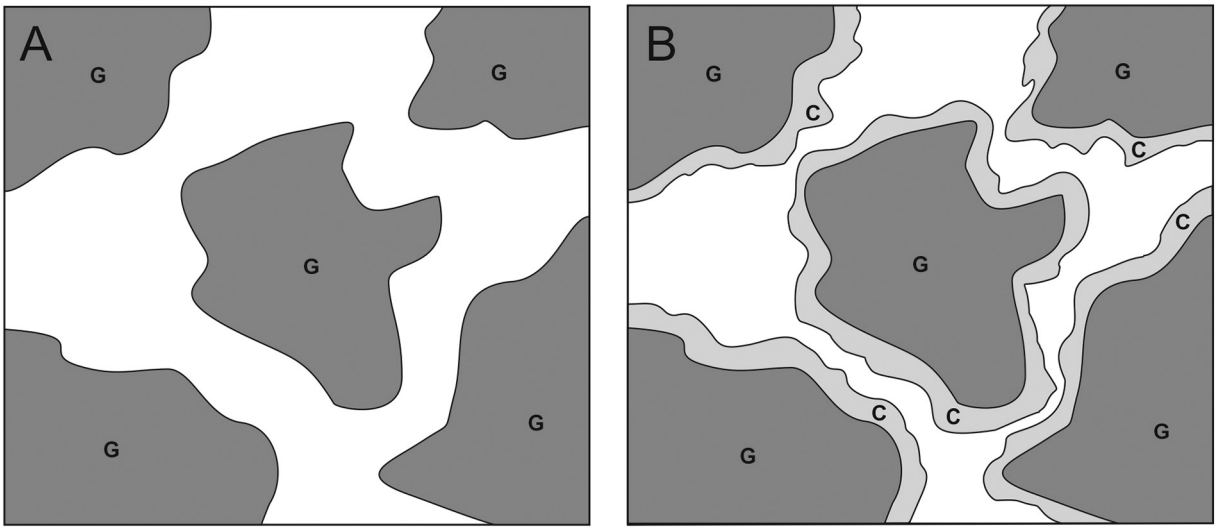

Fig. 4. Influence of clogging on the texture. A) Microscopic scheme without clogging. B) Microscopic scheme with clogging coating the grains, showing how this clogging may block the water flow and how the specific surface area able to exchange cations is increased (i.e. how the CEC is increased and therefore the normalized chargeability). G denotes the gravel grains, C denotes the clogging.

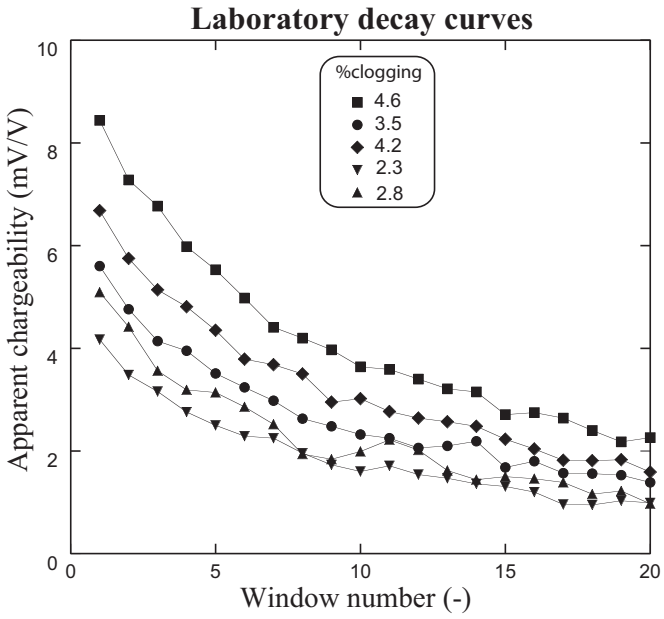

Fig. 5. Apparent chargeability decay curves for 5 of the samples used in the laboratory to test the correlation between the normalized chargeability and the percent of clogging (dry weight). We have sampled the voltage decay over 20 windows W_i (i from 1 to 20). The lines are just guides for the eyes.

14.4 mg/L. are below the threshold of 125 mg/L and a reduction of 75% as set by the Urban Waste Water Treatment Directive #91/271/EEC. The (Biological Oxygen Demand) BOD_5 value is most commonly expressed in milligrams of oxygen consumed per liter of sample during 5 days of incubation at 20C. It is often used as a surrogate of the degree of organic pollution in the contaminated wastewater in the wetland. The mean inlet BOD_5 concentrations in the system ranges from 1020 to 26 mg/L while, at the outlet, it ranges from 90 to 26 mg/L. achieving therefore an average reduction of 90.5%. Outlet values with mean effluent BOD_5 concentrations of 48.5 ± 14.4 mg/L. are above the threshold of 25 mg/L. Note that a reduction between 75% and 90% is set up by the Urban Waste Water Treatment Directive (91/271/EEC). After passing through the treatment wetlands, the pore water goes through two maturation ponds and finally two additional small horizontal subsurface flow treatment wetlands (see sketch in Fig. 1).

The Vedú test site entered into operation in 2002. Since, all the four gravel-based horizontal subsurface flow units have been affected by clogging problems. This issue was minimized by operating regularly some gravel cleaning or substitution, which had the drawback to increase the operational cost of the site.

2.1. Induced polarization

Induced polarization is a non-intrusive geophysical method investigating the ability of porous materials to store reversibly electric charges under the action of an external (primary) electrical field (Vinegar and Waxman, 1984 and Fig. 2). Induced polarization measurements can be performed in time-domain (TDIP) or frequency-domain (FDIP), but in the field TDIP measurements are preferred over FDIP because of the easiness to carried out such measurements with most resistivity meters.

The TDIP approach is sketched in Fig. 3. A box current is injected into the ground using two current electrodes (A and B) over a period T (typically $T = 1$ s) The resulting electrical potential distribution is recorded between two potential electrodes (M and N). In this study we use stainless steel electrodes. When the primary current is shut down, the secondary current decays over time (Fig. 3, Schlumberger, 1920). This decay expresses the fact that the stored electrical charges comes back to their statistical equilibrium position by electro-diffusion (e.g., Revil, 2013b). In order to image the chargeability, the voltage curve is sampled over a series of windows. Then, the polarization data are formed by partial (apparent) chargeabilities (dimensionless but often expressed in mV/V). These partial chargeabilities M_i are obtained by integrating the secondary voltage decay between times t_i and t_{i+1}.

$$M_i = \frac{1}{\psi_0(t_{i+1} - t_i)} \int_{t_i}^{t_{i+1}} \psi(t)dt. \quad (1)$$

In this equation, ψ_0 (in V) denote the potential difference between the voltage electrodes M and N just before the shutdown of the primary current, $\psi(t)$ denote the secondary voltage decay curve associated with ground polarization, $t_i + 1 - t_i$ (s) indicates the duration of the window W_i. During the acquisition, it is recommended to separate the cables for the current injection (containing all the bipoles AB) and the cable used for the voltage measurements (containing all the voltage electrodes

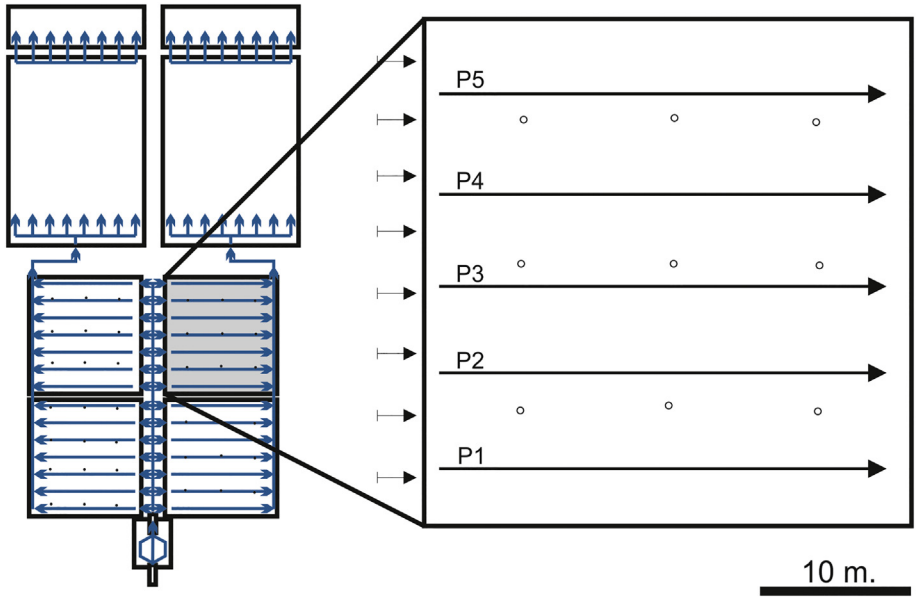

Fig. 6. Location of the five induced polarization profiles (named P1 to P5) over the constructed wetland test site and along the horizontal subsurface flow direction. The small arrows indicate the water inlet and the flow direction from the inlet inward.

Fig. 7. Picture of the constructed wetland investigated in the present paper. The surface flow can be seen along the water inlet as well as the nine piezometers.

MN, see Dahlin and Leroux, 2012). This is done to minimize capacitive and electromagnetics inductive couplings between the wires and to avoid the current electrodes (A and B) polarization, preventing to use them as potential electrodes (M and N).

In order to interpret induced polarization tomograms, we need to describe a fundamental model developed in the past decade and called the dynamic Stern layer model (e.g., Rosen et al., 1993; Revil, 2013b). This model implies that most of the observed polarization in metal-free porous materials is due to the polarization of the Stern layer coating the surface of the grains. This Stern layer forms the inner part of the electrical double layer coating the grains. Considering that an external harmonic electric field $\boldsymbol{E} = \boldsymbol{E}_0 \exp(+i\omega t)$, $\boldsymbol{E}_0$ (V m^{-1}) denotes the amplitude, ω denotes the pulsation frequency (in rad s^{-1}), and t (in s) is applied to the system of interest (core sample or in then field) (primary field), the complex conductivity of the porous rock can be written as

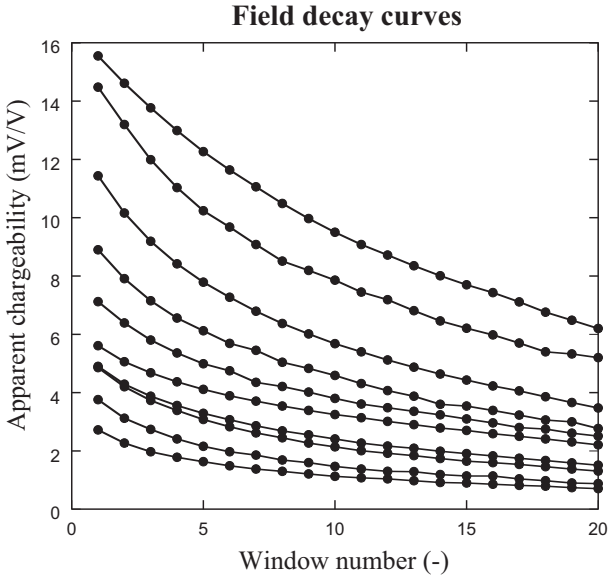

Fig. 8. Selected apparent chargeability decay curves from the field profiles. We have sample the voltage decay over 20 windows like for the laboratory data. The range of the apparent normalized chargeability is reasonably similar in the field and in the laboratory. The lines are just guides for the eyes.

Table 1
Experimental data corresponding to the laboratory experiments.

Experiment	Chargeability M_1(mV/V)	Resistivity (Ohm m)	Clogging Weigh (g)	Gravel weigh (g)	Total weigh (g)	% (weight) Clogging
1	4.17	33.93	19	798.4	817.4	2.32
2	5.09	33.9	33.8	1156.6	1190.4	2.84
3	1.53	41.16	29	1578.5	1607.5	1.80
4	8.44	27.31	50	1032.3	1082.3	4.62
5	5.6	33.57	40.4	1119.5	1159.9	3.48
6	5.93	28.74	26.7	643.3	670	3.99
7	6.68	35.75	28.7	656.8	685.5	4.19
8	5.89	35.27	40.1	890.1	930.2	4.31
9	4.46	30.99	43.3	1086.7	1130	3.83

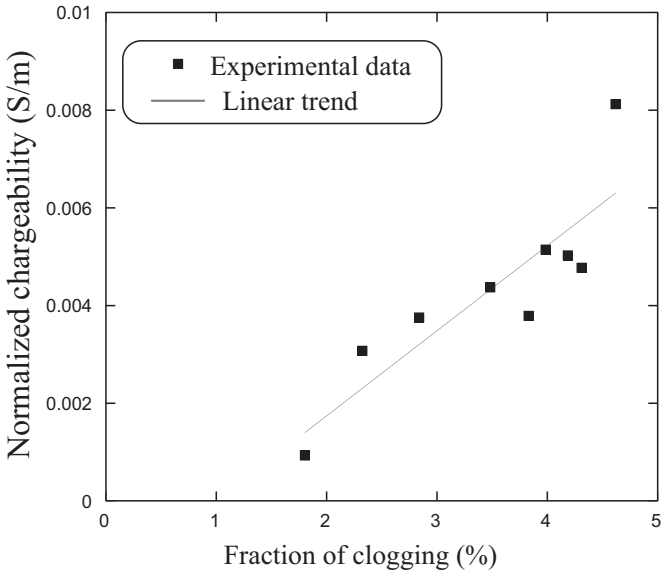

Fig. 9. Normalized chargeability versus percent of clogging graphic from the laboratory samples. The correlation coefficient is $R = 0.873$.

(Revil et al., 2017b)

$$\sigma^*\omega = \sigma_\infty - M_n \int_0^\infty \frac{h\tau}{1 + i\omega\tau^{1/2}} d\tau. \quad (2)$$

The quantity ω denotes the pulsation frequency (expressed in rad s^{-1}), $h(\tau)$ designates a probability density for distribution of the relaxation times associated with charges accumulations at grain scales. In Eq. (1), M_n signifies the normalized chargeability (expressed in S m^{-1}) (Seigel, 1959; Revil et al., 2017a, 2017b) as

$$M \equiv \frac{\sigma_\infty - \sigma_0}{\sigma_\infty}, \quad (3)$$

$$M_n \equiv \sigma_\infty - \sigma_0, \quad (4)$$

where σ_∞ and σ_0 (both in S m^{-1}) denote the instantaneous and DC (Direct Current) conductivity of the porous material, respectively. The quantity σ_∞ corresponds to the conductivity just after the application of the external (primary) electrical field. This "instantaneous conductivity" is somehow difficult to obtain because of electromagnetic coupling effects and is often determined around 100 Hz to 1 kHz. In this situation, all the charge carriers are mobile (Revil et al., 2017a). The quantity σ_0 (S m^{-1}) corresponds to the electrical conductivity of the porous material for a long (typically few minutes) application of the electrical field corresponding to steady-state condition. (Revil et al., 2017a). The DC conductivity is necessarily smaller than the instantaneous conductivity since the charges responsible for the polarization are not available anymore for the conduction process. Extending the bulk conductivity contribution in which is encapsulated Archie's law (Archie, 1942) by including surface conductivity effects, Revil (2013b) obtained the following expressions of the high and low-frequency conductivities,

$$\sigma_\infty = \theta^2\sigma_w + \theta\rho_g B\,\mathrm{CEC}, \quad (5)$$

$$\sigma_0 = \theta^2\sigma_w + \theta\rho_g (B - \lambda)\mathrm{CEC}, \quad (6)$$

respectively. Therefore, the normalized chargeability is given by

$$M_n = \theta\rho_g \lambda\,\mathrm{CEC}. \quad (7)$$

In these equations, θ denotes the volumetric water content (equal to the porosity at saturation), σ_w (in S m^{-1}) is the conductivity of the

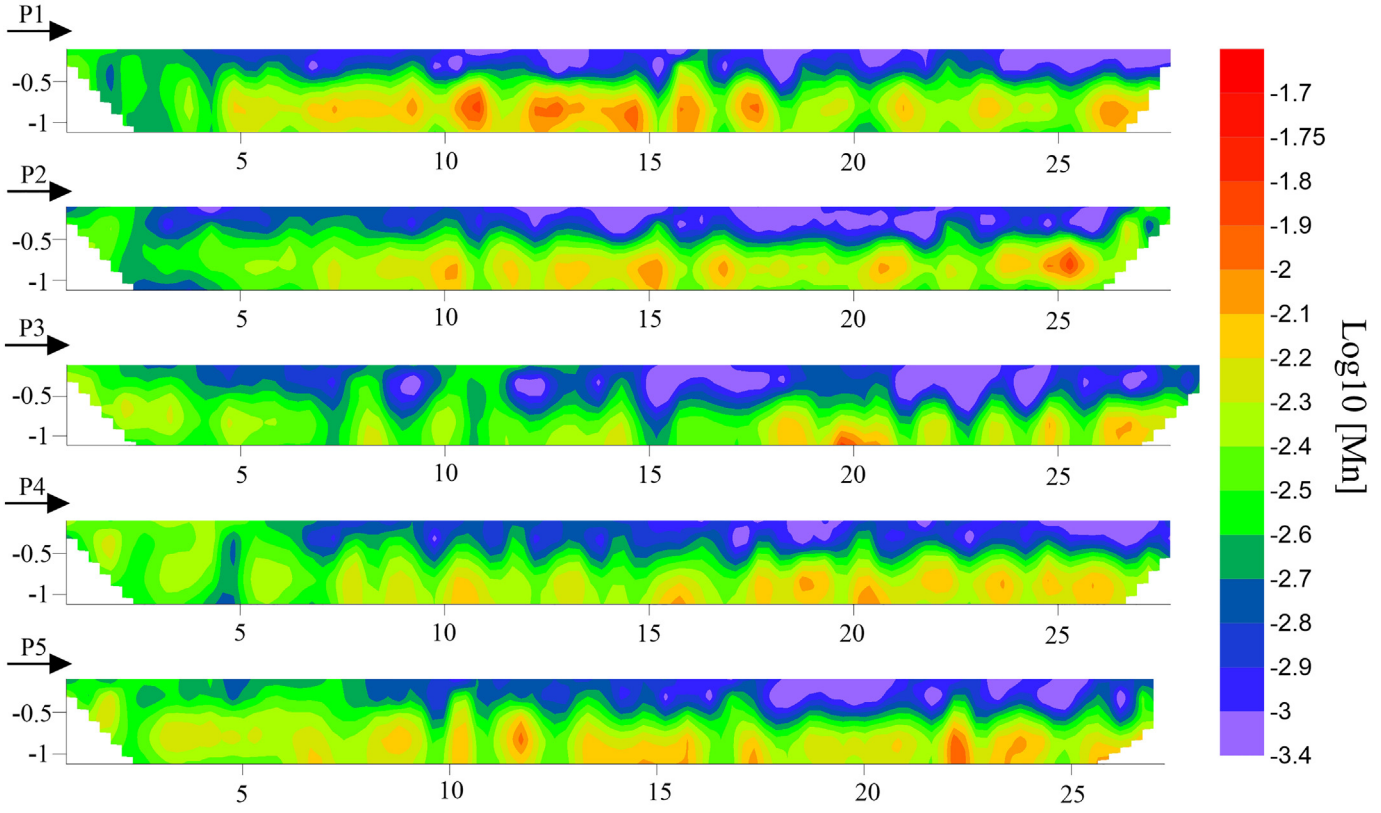

Fig. 10. Normalized chargeability profiles (P1–P5) inverted. The black arrow indicates the water inlet and the flow direction, SW-NE. The water table was initially at a depth of 50 cm.

effluent (liquid pore water solutions), ρ_g designates the grain density (in kg m^{-3}, usually $\rho_g = 2650$ kg m^{-3}), and CEC (C kg^{-1} where C stands for Coulomb) signifies the cation exchange capacity of the material. This CEC corresponds to the density of exchangeable surface sites on the surface of the mineral grains. It is typically measured using titration experiments in which the surface of the grains is exchanged with a cation having a high affinity for the sites populating the mineral surface. It is often expressed in meq/100 g with the conversion 1 meq/100 g = 963.20C kg^{-1}. In Eqs. (3) and (4), B (in m^{2}s^{-1} V^{-1}) denotes the apparent mobility of the counterions for surface conduction. By surface conduction, we mean the conductivity associated with conduction in the electrical double layer coating the surface of the grains. The quantity λ (in m^{2}s^{-1} V^{-1}) symbolizes the apparent mobility of the counterions for the polarization. The surface conductivity corresponds to the last term of Eq. (3) and is written as σs. A dimensionless number R has been introduced by Revil et al. (2017a) $R = \lambda/B$. From Ghorbani et al. (2018), the mobility occuring in the conductivity and normalized chargeability are B (Na^+, 25 °C) $= 3.1 \pm 0.3 \times 10^{-9}$ m^{2}s^{-1} V^{-1} and λ(Na^+, 25 °C) $= 3.0 \pm 0.7 \times 10^{-10}$ m^{2}s^{-1} V^{-1}, and R is typically around 0.09 ± 0.01. In the present paper, we are interested in the dependence of the normalized chargeability with the amount of clogging matter in a horizontal subsurface flow artificial wetland filter. The CEC describes the quantity (in equivalent electrical charge) of the active (exchangeable) sites on the surface of minerals and bacteria per unit mass of minerals and/or bacteria (e.g., Revil, 2012; Revil et al., 2012). The CEC is controlled by the presence of clogging because of the increase of specific surface area caused by the clogging coating the grains (Fig. 4). Therefore, the CEC can be used as a proxy of clogging weight content $\varphi_W \sim$ CEC through the gravel filter. This is the basic assumption used in this paper.

2.2. Laboratory experiments

To test empirically the relation between normalized chargeability and the clogging content φ_W of the gravels, nine one-point induced polarization measurements were carried out on the same horizontal subsurface flow treatment wetland used for the induced polarization profiles acquisition (Fig. 1). The points were located above the profile section closest to each one of the nine piezometers (Fig. 6). We use a Syscal Pro equipment (from IRIS, see www.iris-instruments.com) with a four stainless steel electrode display composed by two current electrodes (AB) and two voltage electrodes (MN) with an AMNB scheme with a 0.5 m spacing and an injection time of 1 s with a dead time of 80 ms before the chargeability sampling and a total of 20 induced polarization windows (Fig. 5). Then the gravel samples from the acquisition points were stored on plastic boxes to analyse them in the laboratory.

In the laboratory, the samples were cleaned with distilled water, this water was decanted three times and filtered to separate the clogging matter and the clean gravels. The gravel and the clogging matter from each sample were dried at 50 °C for three days and then weighed to calculate the % of clogging matter in dry weigh in each gravel sample in relation to the total dry weigh of each sample.

2.3. Field data acquisition

A total of 5 induced polarization profiles (Fig. 6) were acquired in the horizontal subsurface flow treatment wetland studied (Fig. 1); the treatment wetland showing more evident clogging problems with surface flow of the wastewater near the inlet (Fig. 7). Each one of these profiles were composed by 2 concatenated profiles with 72 stainless steel electrodes per profile with a regular spacing of 0.5 m and an injection time of 1 s with a dead time of 80 ms before the chargeability sampling and a total of 20 induced polarization windows (Fig. 8) in order to cover the total length of the treatment wetland without increasing the spacing between electrodes, i.e. without resolution decrease. The resistivity and chargeability measurements have been carried with the Syscal Pro equipment separating the injection and acquisition electrodes to minimize the electromagnetic coupling effects as well electrode polarization issues (Dahlin and Leroux, 2012; Duvillard et al., 2018), a spacing

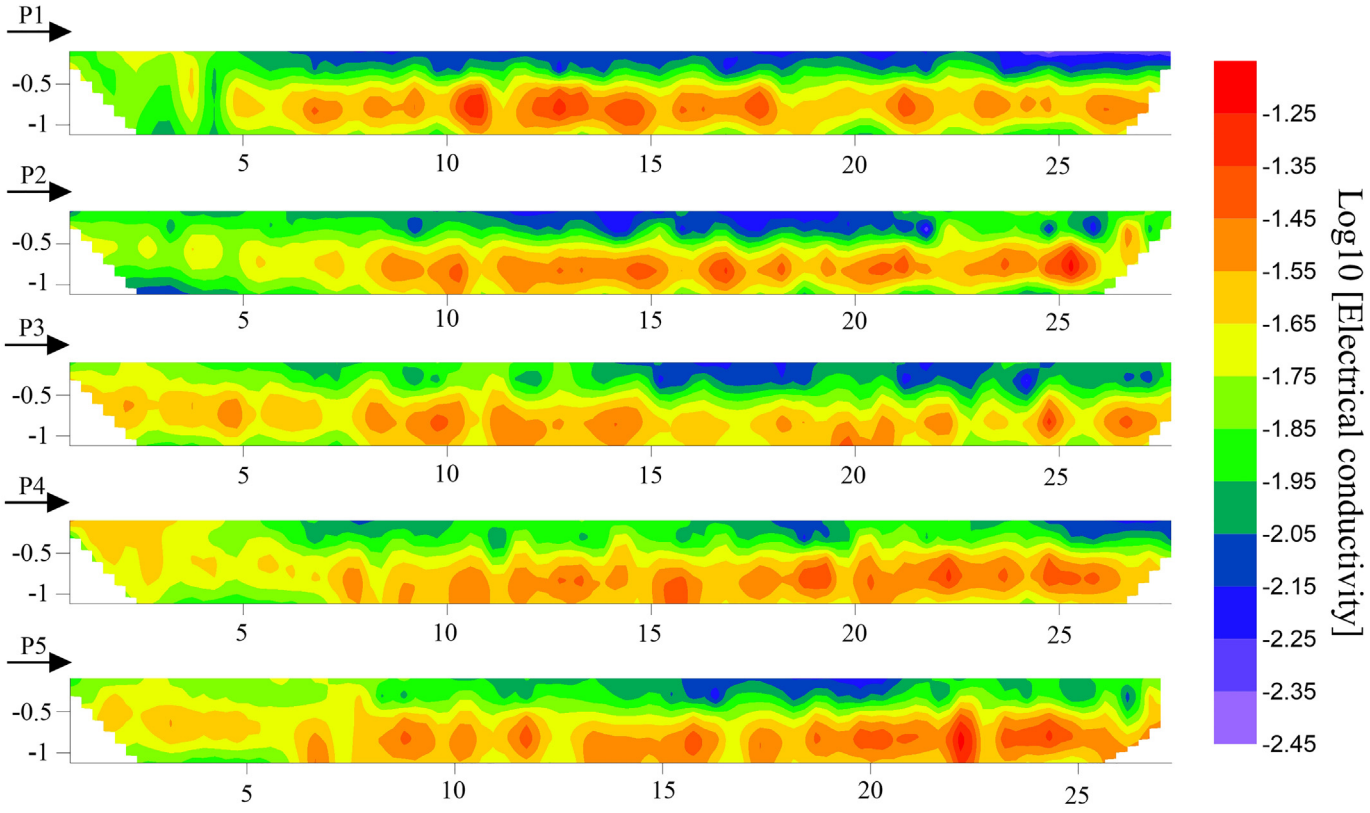

Fig. 11. Conductivity profiles (P1–P5) inverted. The black arrow indicates the water inlet and the flow direction, SW-NE. The water table was initially at a depth of 50 cm.

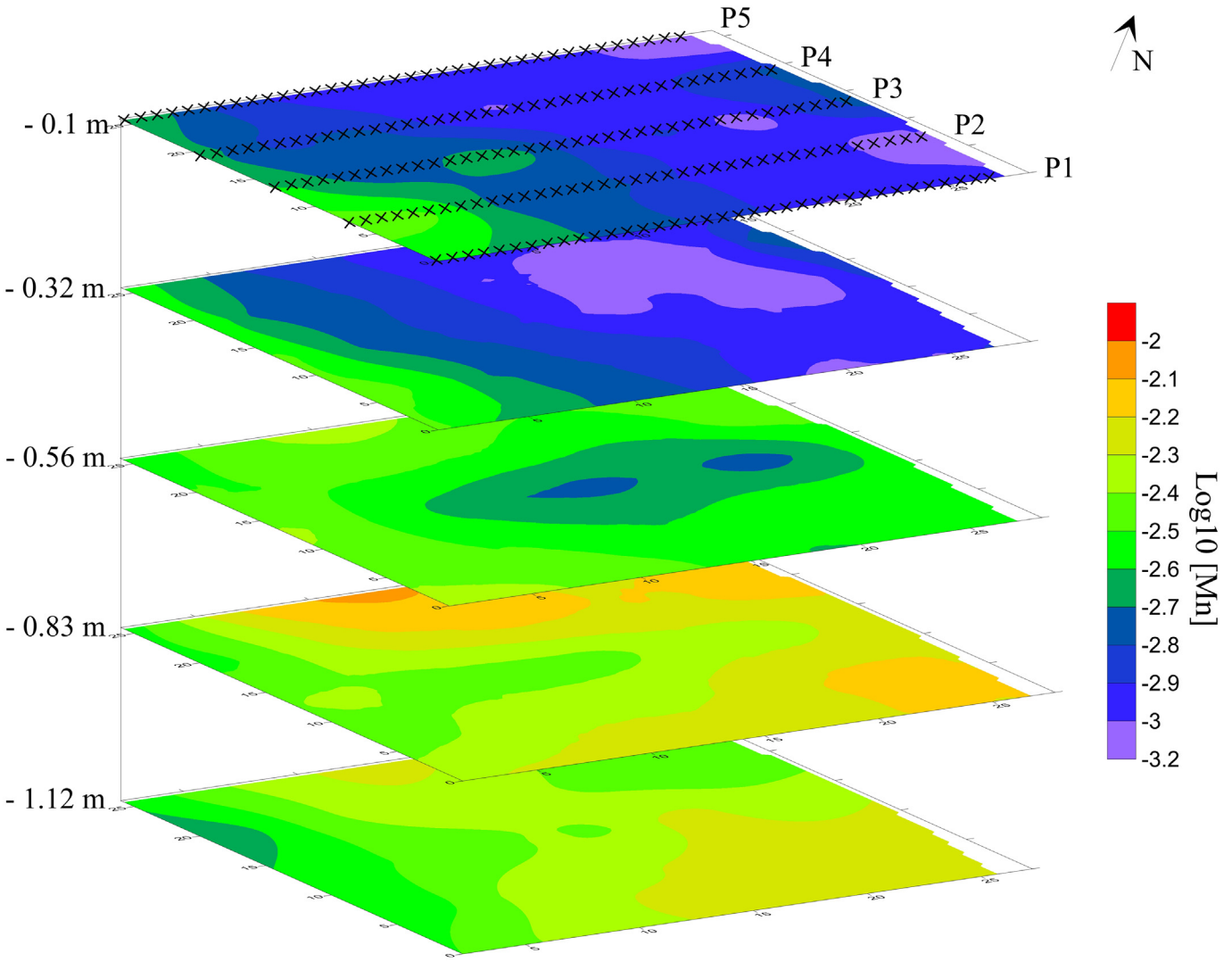

Fig. 12. Normalized chargeability (in S m^{-1}) depth slices. The crosses show the electrode locations at the ground surface. The water table was initially at a depth of 50 cm.

between electrodes of 0.5 m and 20 IP sampling windows (Fig. 8). A multigradient sequence with 234 quadrupoles, an injection time of 1 s with a dead time of 80 ms before the chargeability sampling and a maximum investigation depth of 1.12 m was selected after trial and error tests.

2.4. Inverse modelling

The filtering of the profiles has been done manually by analysing the voltage decay curves obtained in the field. We have discarded an average 19% of the decay curves in which the measurement exhibit erratic behaviours or negative voltage values. With the profiles that have already been filtered, the chargeability data (using only the first window acquired, W1) and resistivity data has been inverted with the Res2Dinv software, thus obtaining the resistivity, conductivity and chargeability of each profile, which allows finally obtaining the normalized chargeability profiles multiplying the chargeability by the conductivity cell by cell.

3. Results

3.1. Laboratory experimental results

The relationship between the normalized chargeability and the percentage of clogging in each sample (calculated in dry weigh of clogging versus the total dry weigh of each sample, see Table 1) displays a direct correlation between these two parameters with a correlation coefficient R of 0.873 (see Fig. 9). We obtain a maximum M_n value of $10^{-2.1}$ S m^{-1} for a sample with $\varphi_W = 4.6\%$ clogging (weight dry) and a minimum value of 10^{-3} S m^{-1} for a sample with $\varphi_W = 1.8\%$ clogging (weight dry), proving that there is an increment on the normalized chargeability (more specifically on the CEC) as a consequence of an increment on the % of clogging in the filter (Fig. 9). From these data we obtain the expression to calculate the % of clogging on each cell from the normalized chargeability profiles as:

$$\varphi_W(\%) = \frac{M_n}{0.0017} + 1. \quad (8)$$

3.2. Results of the induced polarization profiles and clogging estimation

The profiles made show a heterogeneous distribution of the normalized chargeability, associated with the greater or lesser presence of clogging in the gravel filter, which can be subdivided for a better compression into low (<$10^{-2.6}$ S m^{-1}), moderate (>$10^{-2.6}$ S m^{-1} < $10^{-2.2}$ S m^{-1}) and high values (>$10^{-2.2}$ S m^{-1}) (Fig. 8). The electrical conductivity profiles used to calculate the M_n are presented on the Fig. 11. Using the experimental formula that has been obtained (point 3.1) it is possible to obtain profiles of % clogging distribution from the

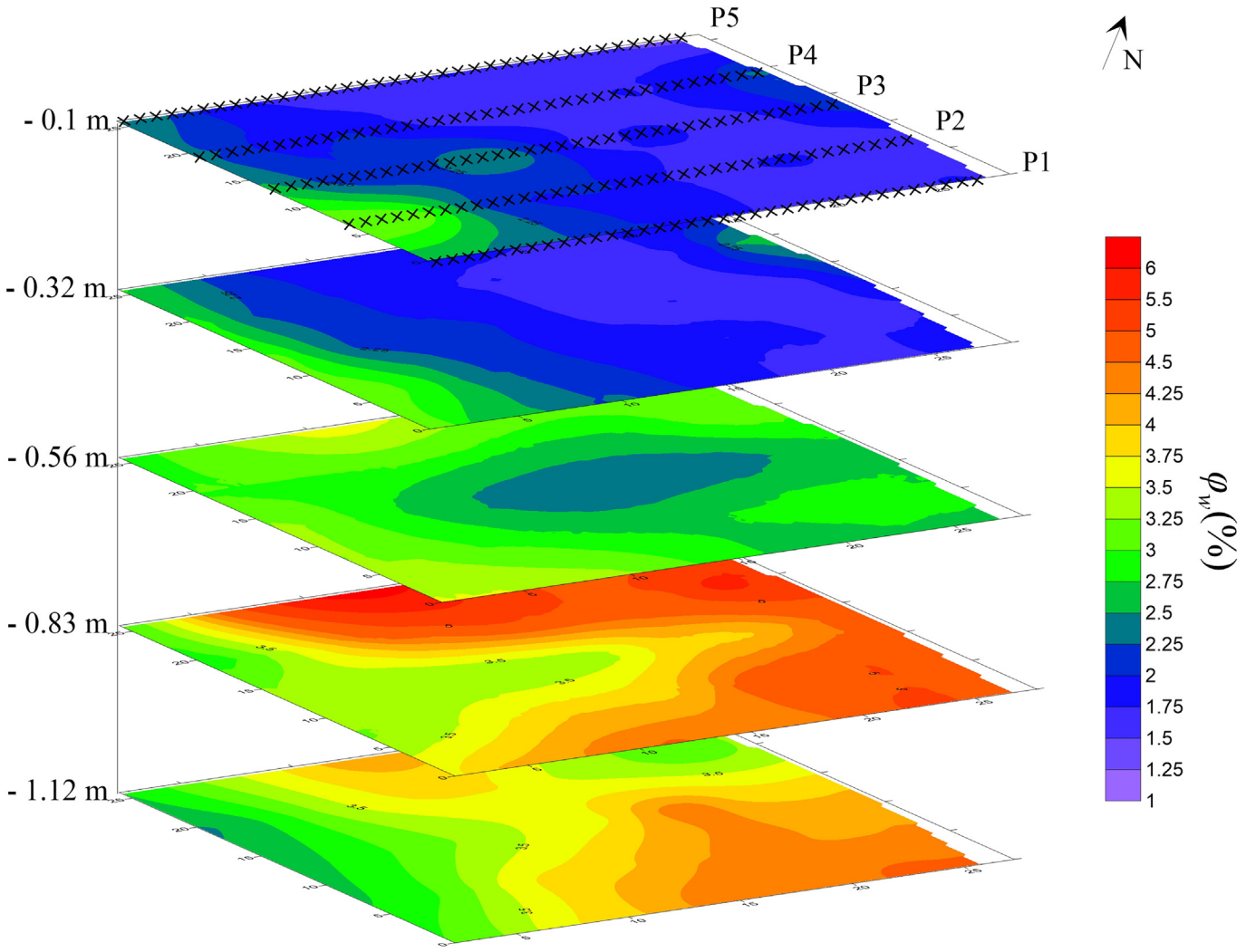

Fig. 13. 3D representation (in depth slices) showing the amount of clogging. This distribution is obtained from the relationship between the normalized chargeability and the percentage of clogging and from the conductivity and chargeability tomograms. The crosses denote the electrode locations at the ground surface. The water table was initially at a depth of 50 cm explaining also the small amount of clogging above this depth.

M_n profiles obtained in the field, which following the criteria applied for M_n can be subdivided into low obstruction (<2.4%), moderate obstruction (>2.7% < 4.7%) and high obstruction (>4.7%). The general pattern of distribution of clogging that can be inferred from the profiles herein presented shows an upper layer with low obstruction, except at the profile start (water inlet) that has moderate obstruction values, that passes to moderate and high obstruction values in depth (Fig. 10).

We also present 5 depth slices of the treatment wetland for M_n (Fig. 12) and percent of clogging (Fig. 13) at depths of −0.1 m, −0.32 m, −0.56 m, −0.83 m and −1.12 m. In the −0.1 m and −0.32 m slices the percent of clogging are similar, with low percent of clogging values in the middle part of the treatment wetland and moderate values at the start (water inlet) and on a zone at the end (water outlet). The −0.56 m-slice shows moderate obstruction values except in its central part following the flow direction were low obstruction values are shown. This trend is also observed in the −0.83 m slice were high obstruction values are dominant in the laterals and at the end of the treatment wetland, but moderate obstruction values are located at the start and at the central part of the treatment wetland. The −1.12 m slice shows, in general, smaller obturation values than the −0.83 m slice, with the higher obturation values still on the laterals of the treatment wetland but occupying a smaller area being the moderate obstruction values dominant.

4. Discussion

The technique herein presented allows to anticipate the critical situation involved in the clogging of the filter since it is able to detect areas where clogging occurs and is concentrated. This method represents a fast, economical, effective way and easily replicable in time, thus giving information on the evolution of this clogging and without need to stop the normal operation of the plant. To give numbers, the present geophysical acquisitions was done with two people in 6 h in a single day. The normalized chargeability depends on the cation exchange capacity (CEC), which will be increased in areas where clogging is present because of the fixation of clay particles and bacteria. We believe (but this would need to be fully proved) that the relationship we have derived between the normalized chargeability and the dry weight of clogging is universal. Typically, a small temperature correction can be applied but would be negligible for practical applications (Revil et al., 2017b).

The depth slices from the 3D tomography give valuable information about the areas where clogging is accumulating in the filter. For the shallow part (slices at depths of 0.1 m and 0.32 m) the condition of the filter is good except close to the outlet and inlet showing higher clogging values. This result is corroborated in the field since it is in these first meters of the filter that surface water flow is observed. The slice corresponding to a depth of 0.56 m shows moderate clogging

values except in the central part of the filter, where they are rather low. Two observations can be done. The degree of clogging increases with depth and clogging is not homogeneously distributed, which generates preferential water flow paths. The highest clogging is shown at a depth of 0.83 m, on the sides of the filter giving rise to a preferred water flow zone at the beginning and through the center of the filter. The deepest slice at 1.12 m displays heterogeneity in the clogging distribution. In turn this leads to preferential flow zones. The inferences obtained from the analysis of the geophysical data can be used to optimize the areas of the filter to be treated first in an efficient way. Time-lapse geophysical measurements (with electrodes let in the field) can be used to monitor the occurrence of clogging over time, which can be useful to anticipate potential problems such as surface water flow or the creation of areas without flow in depth. It is possible to plan a partial substitution of the gravels, affecting only the area of high clogging values, thus reducing both the economic cost of the operation and the time to stop the system.

5. Conclusions

Time-domain induced polarization is used for the first time to image clogging distribution of a gravel filter from a horizontal subsurface flow treatment wetland. Experimental data performed on the laboratory demonstrates the linear relationship between the normalized chargeability and the amount of clogging in the gravel filter because of the substantial increase of the cation exchange capacity caused by clogging coating these grains. This is expected since clogging contains fine particles and bacteria characterized by high cation exchange capacity. Therefore, we were able to convert the 3D normalized chargeability tomogram obtained with the field data into a 3D distribution of the percent clogging. This method allows to identify the zones were the clogging has accumulated trough the filter and therefore predict preferential flow paths and dead flow zones. This is an important task to plan preventive measures and anticipate the filter obstruction that may decreases the effectiveness of the waste water treatment system.

CRediT authorship contribution statement

R. Garcia-Artigas: Methodology, Writing - original draft, Writing - review & editing. **M. Himi:** Data curation, Supervision, Writing - review & editing. **A. Revil:** Conceptualization, Formal analysis, Methodology, Writing - original draft, Writing - review & editing. **A. Urruela:** Methodology, Writing - review & editing. **R. Lovera:** Methodology, Writing - review & editing. **A. Sendrós:** Methodology, Writing - review & editing. **A. Casas:** Methodology, Writing - review & editing. **L. Rivero:** Methodology, Writing - review & editing.

Declaration of competing interest

The authors declare that they have no known competing financial interests or personal relationships that could have appeared to influence the work reported in this paper.

Acknowledgements

This work is supported by Water Research Institute (IdRA) from the University of Barcelona and by the predoctoral grant APIF from the University of Barcelona. We also thank the help and the support provided in the field by both Angel Lázaro and Montse Palomes from Aigües de Catalunya. We thank the Associate Editor, Jose Julio Ortega-Calvon and four referees for their fruitful and constructive comments.

References

Abed, S.N., Almuktar, S.A., Scholz, M., 2017. Remediation of synthetic greywater in mesocosm - scale floating treatment wetlands. Ecol. Eng. 102, 303–319. https://doi.org/10.1016/j.ecoleng.2017.01.043.

Archie, G.E., 1942. The electrical resistivity log as an aid in determining some reservoir characteristics. Transactions of the AIME. Society of Petroleum Engineers 146, 54–62. https://doi.org/10.2118/942054-G.

Dahlin, T., Leroux, V., 2012. Improvement in time-domain induced polarization data quality with multi-electrode systems by separating current and potential cables. Near Surface Geophysics 10, 545–565. https://doi.org/10.3997/1873-0604.2012028.

Dotro, G., Langergraber, G., Molle, P., Nivala, J., Puigagut, J., Stein, O.R., von Sperling, M., 2017. Treatment Wetlands; Biological Wastewater Treatment Series. 7. IWA Publishing, London, UK, p. 172 2017. ISBN 9781780408774. https://doi.org/10.2166/9781780408774.

Duvillard, P.A., Revil, A., Soueid Ahmed, A., Qi, Y., Coperey, A., Ravanel, L., 2018. Three-dimensional electrical conductivity and induced polarization tomography of a rock glacier. J. Geophys. Res. 123, 9528–9554. https://doi.org/10.1029/2018JB015965.

Ghorbani, A., Revil, A., Coperey, A., Soueid Ahmed, A., Roque, S., Heap, M.J., Grandis, H., Viveiros, F., 2018. Complex conductivity of volcanic rocks and the geophysical mapping of alteration in volcanoes. J. Volcanol. Geotherm. Res. 357, 106–127. https://doi.org/10.1016/j.jvolgeores.2018.04.014.

Headley, T.R., Tanner, C.C., 2011. Constructed wetlands with floating emergent macrophytes: an innovative stormwater treatment technology. Crit. Rev. Environ. Sci. Technol. 42, 2261–2310. https://doi.org/10.1080/10643389.2011.574108.

Kadlec, R.H., Wallace, S.D., 2009. Treatment Wetlands. 2nd ed. CRC Press, Boca Raton, FL, USA 9781566705264, p. 2009.

Kim, B., Forquet, N., 2016. Pore-scale observation of deposit within the gravel matrix of a vertical flow constructed wetland. Environ. Technol. 37, 3146–3150. https://doi.org/10.1080/09593330.2016.1178334.

Knowles, P., Dotro, G., Nivala, J., García, J., 2011. Clogging in subsurface-flow treatment wetlands: occurrence and contributing factors. Ecol. Eng. 37, 99–112. https://doi.org/10.1016/j.ecoleng.2010.08.005.

Licciardello, F., Aiello, R., Alagna, V., Iovino, M., Ventura, D., Cirelli, G.L., 2019. Assessment of clogging in constructed wetlands by saturated hydraulic conductivity measurements. Water Sci. Technol. 79, 314–332. https://doi.org/10.2166/wst.2019.045.

Martinez-Carvajal, G.D., Oxarango, L., Adrien, J., Molle, P., Forquet, N., 2019. Assessment of X-ray computed tomography to characterize filtering media from vertical flow treatment wetlands at the pore scale. Sci. Total Environ. 658, 178–188. https://doi.org/10.1016/j.scitotenv.2018.12.119.

Martinez-Carvajal, G.D., Oxarango, L., Clément, R., Molle, P., Forquet, N., 2020. Assessment of spatial representativity of X-ray tomography to study vertical flow treatment wetlands. Sci. Total Environ. 713, 136510. https://doi.org/10.1016/j.scitotenv.2020.136510.

Marzo, A., Ventura, D., Cirelli, G.L., Aiello, R., Vanella, D., Rapisarda, R., Barbagallo, S., Consoli, S., 2018. Hydraulic reliability of a horizontal wetland for wastewater treatment in Sicily. Sci. Total Environ. 636, 94–106. https://doi.org/10.1016/j.scitotenv.2018.04.228.

Matos, M.P., von Sperling, M., Matos, A.T., Miranda, S.T., Souza, T.D., Costa, L.M., 2017. Key factors in the clogging process of horizontal subsurface flow constructed wetlands receiving anaerobically treated sewage. Ecol. Eng. 106, 588–596. https://doi.org/10.1016/j.ecoleng.2017.06.013.

Matos, M.P., von Sperling, M., Matos, A.T., 2018. Clogging in horizontal subsurface flow constructed wetlands: influencing factors, research methods and remediation techniques. Rev. Environ. Sci. Biotechnol. 17, 87–107. https://doi.org/10.1007/s11157-018-9458-1.

Matos, M.P., von Sperling, M., Matos, A.T., Aranha, P.R.A., Santos, M.A., Pessoa, F.D.B., Viola, P.D.D., 2019. Clogging in constructed wetlands: indirect estimation of medium porosity by analysis of ground-penetrating radar images. Sci. Total Environ. 676, 333–342. https://doi.org/10.1016/j.scitotenv.2019.04.168.

Nivala, J., Rousseau, D.P.L., 2009. Reversing clogging in subsurface-flow constructed wetlands by hydrogen peroxide treatment: two case studies. Water Sci. Technol. 59, 2037–2046. https://doi.org/10.2166/wst.2009.115.

Nivala, J., Knowles, P., Dotro, G., García, J., Wallace, S., 2012. Clogging in subsurface-flow treatment wetlands: measurement, modeling and management. Water Res. 46, 1625–1640. https://doi.org/10.1016/j.watres.2011.12.051.

Pedescoll, A., Corzo, A., Álvarez, E., García, J., Puigagut, J., 2011. The effect of primary treatment and flow regime on clogging development in horizontal subsurface flow constructed wetlands: an experimental evaluation. Water Res. 45, 3579–3589. https://doi.org/10.1016/j.watres.2011.03.049.

Pucher, B., Langergraber, G., 2019. The state of the art of clogging in vertical flow wetlands. Water 11, 2400. https://doi.org/10.3390/w11112400.

Puigagut, J., Villaseñor, J., Salas, J.J., Bécares, E., García, J., 2007. Subsurface-flow constructed wetlands in Spain for the sanitation of small communities: a comparative study. Ecol. Eng. 30 (4), 312–319. https://doi.org/10.1016/j.ecoleng.2007.04.005.

Ranieri, E., 2012. Chromium and nickel control in full- and small-scale subsuperficial flow constructed wetlands. Soil Sediment Contam. 21 (7), 802–814. https://doi.org/10.1080/15320383.2012.691133.

Ranieri, E., Young, T.M., 2012. Clogging influence on metals migration and removal in subsurface flow constructed wetlands. J. Contam. Hydrol. 129–130, 38–45. https://doi.org/10.1016/j.jconhyd.2012.01.002.

Ranieri, E., Fratino, U., Petrella, A., Torretta, V., Rada, E.C., 2016. *Ailanthus altissima* and *Phragmites australis* for chromium removal from a contaminated soil. Environ. Sci. Pollut. Res. 23 (16), 15983–15989. https://doi.org/10.1007/s11356-016-6804-0.

Revil, A., 2012. Spectral induced polarization of shaly sands: influence of the electrical double layer. Water Resour. Res. 48, W02517. https://doi.org/10.1029/2011WR011260.

Revil, A., 2013a. Effective conductivity and permittivity of unsaturated porous materials in the frequency range 1 mHz–1GHz. Water Resour. Res. 49, 306–327. https://doi.org/10.1029/2012WR012700.

Revil, A., 2013b. On charge accumulations in heterogeneous porous materials under the influence of an electrical field. Geophysics 78 (4), D271–D291. https://doi.org/10.1190/geo2012-0503.1.
Revil, A., Florsch, N., 2010. Determination of permeability from spectral induced polarization data in granular media. Geophys. J. Int. 181, 1480–1498. https://doi.org/10.1111/j.1365-246X.2010.04573.x.
Revil, A., Atekwana, E., Zhang, C., Jardani, A., Smith, S., 2012. A new model for the spectral induced polarization signature of bacterial growth in porous media. Water Resour. Res. 48, W09545. https://doi.org/10.1029/2012WR011965.
Revil, A., Ahmed, A. Soueid, Jardani, A., 2017a. Self-potential: a non-intrusive ground water flow sensor. J. Environ. Eng. Geophys. 22 (3), 235–247. https://doi.org/10.2113/JEEG22.3.235.
Revil, A., Coperey, A., Shao, Z., Florsch, N., Fabricius, I.L., Deng, Y., Delsman, J.R., Pauw, P.S., Karaoulis, M., de Louw, P.G.B., van Baaren, E.S., Dabekaussen, W., Menkovic, A., Gunnink, J.L., 2017b. Complex conductivity of soils. Water Resour. Res. 53, 7121–7147. https://doi.org/10.1002/2017WR020655.
Rosen, L., Baygents, J., Saville, D., 1993. The interpretation of dielectric response measurements on colloidal dispersions using the dynamic stern layer model. J. Chem. Phys. 98, 4183–4194. https://doi.org/10.1063/1.465108.
Schlumberger, C., 1920. Study of Underground Electrical Prospecting (99 pp. Paris).
Seigel, H.O., 1959. Mathematical formulation and type curves for induced polarization. Geophysics 24, 547–565. https://doi.org/10.1190/1.1438625.
Tapias, J.C., Himi, M., Lovera, R., Folch, M., Font, X., Casas, A., 2013. Evaluación mediante tomografia de resistividad eléctrica de las propiedades hidráulicas de la zona saturada y no-saturada de humedales artificiales para el tratamiento de agua residual. Estudios de la Zona no Saturada del Suelo 11, 51–55.
Vera, I., García, J., Sáez, K., Moragas, L., Vidal, G., 2011. Performance evaluation of eight years experience of constructed wetland systems in Catalonia as alternative treatment for small communities. Ecol. Eng. 37, 364–371. https://doi.org/10.1016/j.ecoleng.2010.11.031.
Vinegar, H.J., Waxman, M.H., 1984. Induced polarization of Shaly Sands. Geophysics 49, 1267–1287. https://doi.org/10.1190/1.1441755.
Vymazal, J., 2005. Horizontal sub-surface flow and hybrid constructed wetlands systems for wastewater treatment. Ecol. Eng. 25, 478–490.
Vymazal, J., 2011. Constructed wetlands for wastewater treatment: five decades of experience. Environ. Sci. Technol. 45, 61–69. https://doi.org/10.1016/j.ecoleng.2005.07.010.
Vymazal, J., 2014. Constructed wetlands for treatment of industrial wastewaters: a review. Ecol. Eng. 73, 724–751. https://doi.org/10.1016/j.ecoleng.2014.09.034.
Zhang, C., Revil, A., Fujita, Y., Munakata-Marr, J., Redden, G., 2014. Quadrature conductivity: a quantitative indicator of bacteria abundance in porous media. Geophysics 79 (6), D363–D375. https://doi.org/10.1190/GEO2014-0107.1.